

# Autonomous Satellite Rendezvous and Docking Using LIDAR and Model Based Vision

Piotr Jasiobedzki<sup>1</sup>, Stephen Se<sup>1</sup>, Tong Pan<sup>1</sup>, Manickam Umasuthan<sup>1</sup>, Michael Greenspan<sup>2</sup>

<sup>1</sup>MDA Space Missions, 9445 Airport Road, Brampton, ON, Canada L6S 4J3

<sup>2</sup>Dept. of Electrical & Computer Engineering, School of Computing, Queen's University, Canada

## ABSTRACT

Servicing satellites on-orbit requires ability to rendezvous and dock by an unmanned spacecraft with no or minimum human input. Novel imaging sensors and computer vision technologies are required to detect a target spacecraft at a distance of several kilometers and to guide the approaching spacecraft to contact. Current optical systems operate at much shorter distances, provide only bearing and range towards the target, or rely on visual targets.

Emergence of novel LIDAR technologies and computer vision algorithms will lead to a new generation of rendezvous and docking systems in the near future. Such systems will be capable of autonomously detecting a target satellite at a distance of a few kilometers, estimating its bearing, range and relative orientation under virtually any illumination, and in any satellite pose.

At MDA Space Missions we have developed a proof-of-concept vision system that uses a scanning LIDAR to estimate pose of a known satellite. First, the vision system detects a target satellite, and estimates its bearing and range. Next, the system estimates the full pose of the satellite using a 3D model. Finally, the system tracks satellite pose with high accuracy and update rate. Estimated pose provides information where the docking port is located even if the port is not visible and enables selecting more efficient flight trajectory.

The proof-of-concept vision system has been integrated with a commercial time-of-flight LIDAR and tested using a moving scaled satellite replica in the MDA Vision Testbed

**Keywords:** LIDAR, model based vision, pose estimation, satellite rendezvous and docking

## 1 INTRODUCTION

There are a number of space operations that require the ability to rendezvous and dock by an unmanned spacecraft with no or with minimum human input, including: servicing satellites; assembly of large space structures in Earth orbit; and transfer of Martian soil samples from a lander to a return spacecraft on the Mars orbit, as part of a sample return mission. Novel imaging sensors and computer vision technologies are required to detect a target spacecraft at a distance of several kilometers in an arbitrary orientation and to guide the approaching spacecraft to contact with the docking port. Current rendezvous and docking systems operate at much shorter distances, provide only bearing and range towards the target, or rely on retro-reflectors or visual targets and require that the target be oriented towards the approaching spacecraft, and may operate only during eclipse.

The emergence of novel LIDAR technologies and computer vision algorithms will lead to a new generation of rendezvous and docking systems in the near future. Such systems will be capable of autonomously detecting a target satellite at a distance of a few kilometers, and estimating its bearing, range and relative 6 degree of freedom orientation under virtually any illumination, and in any satellite pose and configuration. This will enable the execution of fuel efficient approach trajectories and reliable operations under any illumination conditions, as well as enabling inspection during fly around and safe station-keeping.

## 2 AUTONOMOUS SATELLITE RENDEZVOUS AND DOCKING

Autonomous rendezvous and docking typically requires multiple systems to complete the operation, as one system will not be suitable for the whole range of operations. Optical line-of-sight systems are expected to provide measurements of a relative position of a target spacecraft at distances below several km and continue until the final contact [6]. Initially, only the bearing and range are necessary for the relative navigation. At a distance of 30-50 m information about the relative target spacecraft attitude (i.e., pose) can be used by the servicer trajectory to align itself with a docking port on the target. In addition to the servicer guidance, the optical sensor can be used to collect images and 3D data of the target

spacecraft. This operation is performed when both spacecrafts are stationary or during a fly-around at a distance of 20-100m.

Manual and automated rendezvous and docking in space has been performed since the 1960s. An overview of earlier missions and technologies has been presented in [6, 21]. Two optical technologies currently used for space rendezvous and docking are cameras and scanning laser rangefinders. The camera based systems typically operate at ranges of up to 100m and the maximum range is limited by a trade-off between the camera image resolution and field of view, and the size and separation of visual targets. Scanning laser rangefinders use beam steering devices to direct a laser beam to objects in the scene and rely on either a triangulation principle, a measure the phase shift (continuous wave), or the time (time-of-flight devices with pulsed laser) of the returned signal. The triangulation based systems operate at the highest acquisition rates but their effective distance is limited to approximately 15 m. The continuous wave systems operate at rates of  $10^5$  measurements per second but only at the distances of up to 10s of meters. The time-of-flight systems operate at lower rates of  $10^4$  points per second but at much longer distances of up to several kms.

The Video Guidance Sensor (VGS) comprises laser diodes to illuminate a target consisting of multiple retro-reflectors, a CCD camera to capture images, and a processor to estimate the relative position and orientation of the target [13]. VGS was tested in Shuttle missions, and operates from 110 meters down to 0.5 meters estimating the pose at 5 Hz.

The Rendezvous Radar (RVR) was used in rendezvous during the ETS-VII mission [11]. RVR can operate at the range from 0.3 m to 660 m and measures distance and bearing towards a reflector mounted on the target satellite.

The Laser Camera System (LCS) [23] was used during a Shuttle mission to collect 3D images and demonstrate tracking of visual targets on one of the ISS modules. This system is based on the active triangulation principle [2] and can be used at distances from 1 to 30 m.

The Trajectory Control Sensor (TCS) is a time-of-flight scanning rangefinder that is used together with other sensors during the manned rendezvous and proximity operations of the Shuttle. TCS tracks a retro-reflector and fuses these measurements with inertial sensors [4].

The Rendezvous and Docking Sensor (RVS) has been developed for automated docking and berthing of the European Automated Transfer Vehicle (ATV) and the Japanese H II Transfer Vehicle (HTV) with the International Space Station (ISS) [22]. RVS uses the time-of-flight principle, operates at ranges from 1 to 1,000 m and estimates the pose by tracking retro-reflectors on the ISS during the approach.

### **3 LIDAR BASED RENDEZVOUS SYSTEMS FOR SPACE**

Reducing the number of sensors necessary to cover the required range of distances (preferably to one) has significant benefits due the reduced launch mass and volume, and lower power requirements. Terrestrial scanning LIDARs provide accurate 3D measurements at distances from meters to hundreds of meters [ILRIS 3D] and in space this distance extends to kilometers [18]. Therefore this technology seems to be the most suitable for use in long range rendezvous and docking systems.

The data from the scanning rangefinder must be processed by a vision system to compute the information, such as distance, bearing, pose, that is required by the Guidance, Navigation and Control unit of the autonomous service spacecraft.

#### **3.1 Operational ranges**

Properties of the scanning LIDAR (e.g., laser beam divergence, field of view, resolution and accuracy), target satellite size and shape, and the relative distance determine what data is available from the sensor for processing by the vision system. Depending upon the distance range, different information is required for servicer navigation, and so different algorithms have to be used at different ranges. Figure 1 illustrates three operational ranges defined using the beam divergence and the LIDAR field of view.

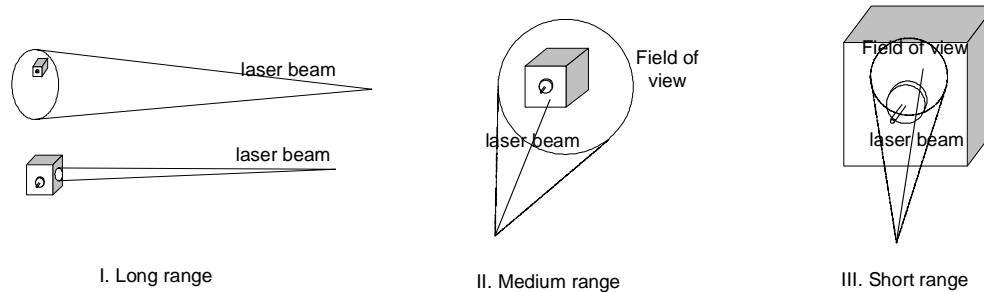


Figure 1: Operational ranges.

At the long range, due to the laser beam divergence, the whole spacecraft may be either within the beam or only a small number of non-overlapping range measurements may be obtained. This does not allow resolving surface features and the vision system may compute only simple geometric 3D moments for all returns. Calculation of a 3D centre of gravity allows estimating bearing and range to the spacecraft. If the number of individual measurements numbers is close to a hundred, then it is possible to compute higher geometrical moments, which allow determining coarse spacecraft orientation.

At the medium range the target spacecraft is fully contained within the LIDAR field of view. Sufficient data resolution allows the detection and reconstruction of surface features as more than  $10^4$  non-overlapping data points ( $100 \times 100$ ) will be available. The vision system may compute position and orientation of the target spacecraft using either features distributed on the spacecraft or the complete spacecraft model.

At the short range the LIDAR field of view restricts the visibility to only a portion of the target spacecraft. It then becomes necessary to rely on local features, e.g., on or around the docking interface. At this range the vision system computes the position and orientation of a docking interface on the target spacecraft

### 3.2 Pose estimation

The systems that have flown in space to date use retro-reflectors or optical targets to provide an easily detectable signal. Such signals (laser beam reflections or images with distinctive high contrast features) can be processed at rates of 10 Hz or greater using simple processing hardware. However, using targets imposes restrictions on the rendezvous and docking operations, and approach trajectories, and may require control over the target spacecraft. In some cases it is necessary to approach the target spacecraft from any direction or perform a fly around operation using visual feedback [12]. The use of optical targets also introduces a failure mode when one or more targets may not be detectable due to damage. New technologies are currently under development that will remove the current need for retro-reflectors or visual targets by using modern computer vision methods that rely on 3D models of observed satellites.

Kawano [17] describes a vision system prototype that uses the Laser Range Finder (LRF) to detect a planar side of a satellite mockup with a ring shaped motor interface. LRF operates at the range from 1 to 100 m and scans the full field of view with resolution of  $256 \times 256$  at a rate of 2 Hz. The detection algorithm uses a Hough transform to detect a dominant plane (the planar side of a cube shaped satellite), maps 3D points into the local coordinate system and detects the ring. The prototype system was tested with a satellite mockup and a sun simulator in laboratory conditions.

For complex shapes that cannot be decomposed into planar surfaces it is necessary to store a 3D representation of the target satellite and match it with range measurements. Geometrical probing [8] can be used to preprocess a representation of the object, which is then used for efficient and reliable pose determination. Alternatively, local 3D features can be detected using special operators such as tripod operator [5, 20], spin images shapes [16], or point signatures [3]. After matching these features with a stored model the resulting pose can be computed by finding the rigid body transformation between the features and the model.

If the previous pose of the satellite is known from earlier iterations, then the problem of estimating the pose can be simplified by restricting the search to solutions that are close the previous pose. In this cases, an Iterative Closest Point (ICP) algorithm [1] can be used to align the satellite model with the 3D data [14, 24]. An alternative is the Bounded Hough Transform (BHT), which searches the 6 dimensional solution space in the vicinity of the last pose and can estimate the pose efficiently and reliably in sparse data, even in the presence of noise and outliers [9].

## 4 MDA MODEL BASED POSE ESTIMATION SYSTEM

This paper describes the research and development of model based pose estimation algorithms that are suitable for the medium and short operating ranges described above. A space qualified LIDAR based rendezvous system, also developed at MDA and scheduled for launch in 2005, implements the complimentary long range functionality, and is described in [18] in this same volume.

Experiments with the model based system have been performed using physical replicas of satellites and calibration objects at the MDA Vision Testbed. A rendering of Radasat-2 and a scaled replica are shown in Figure 2. A virtual model of the same satellite was used in simulations.

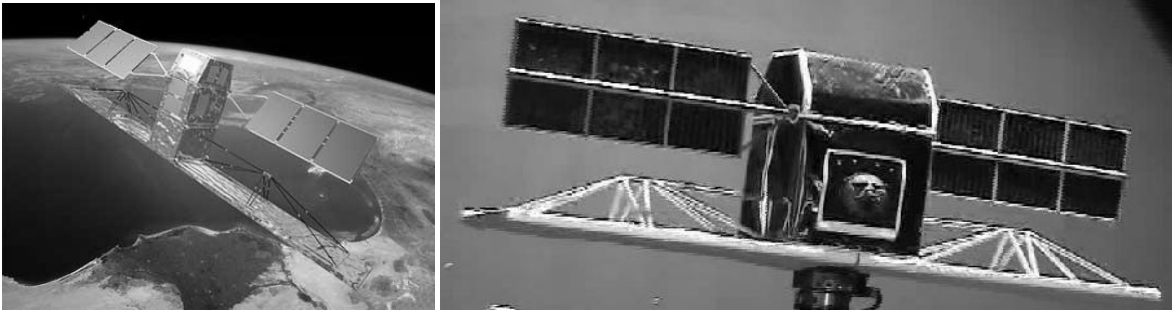


Figure 2: Radasat-2 (left) and its replica used in experiments at MDA (right)

### 4.1 System architecture

The system architecture is shown in Figure 3. A request for a LIDAR scan including the scan window size, location with the LIDAR field of view, resolution, and scan pattern, is sent to a LIDAR unit. The LIDAR returns measurements encoded as range, and elevation and azimuth angles, with additional status information. This data is then filtered and converted into Cartesian coordinates for further processing. First, the Pose Acquisition module is invoked; this module operates on a point cloud, and does not require any prior knowledge of the spacecraft distance and relative orientation. This module computes an initial relative pose using a model of the target spacecraft. The computed pose is next sent to a Target Tracker module that maintains a current pose estimate in subsequent data frames and selects new scan windows. These scan windows are mapped into LIDAR coordinates and a request for a new scan is sent to the LIDAR. The Pose Tracking module uses the current estimate of the target pose, the new 3D data, and a model of the target satellite to compute a new pose at each frame. Pose Tracking operates at higher rates and is more accurate than Pose Acquisition, but it does require an initial value. The pose estimate is used by the Tracker module to update the relative pose state, and the estimated pose, which includes a measurement confidence and system status, is then sent to a Guidance, Navigation, and Control module via a suitable communication channel. This channel is also used to send commands.

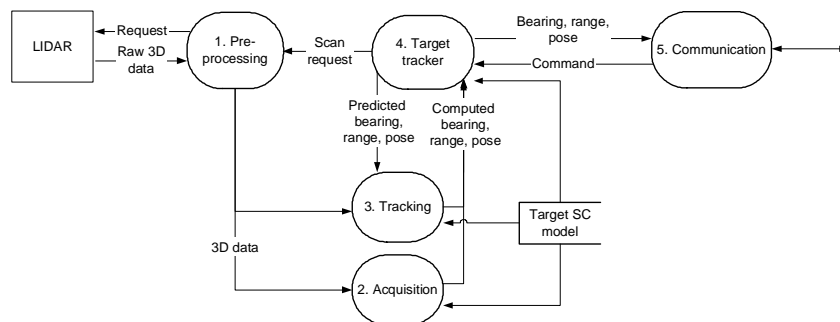


Figure 3: Architecture of the model based pose estimation system

### 4.2 Scanning LIDAR

In recent experiments we have interfaced a commercial terrestrial LIDAR system, the ILRIS 3D from Optech [19] with our vision system. ILRIS 3D uses a class I laser with a beam divergence of 0.17 mrad and a sampling rate of 2,000 points/second. The range is from 3 to 350 m (at 4% reflectivity) and 3 to 800 m (at 20% reflectivity), and the depth

resolution is 3 mm. The horizontal and vertical field of view is 40 degrees. ILRIS 3D can be controlled remotely via Ethernet, and multiple scan windows with a programmable density and a raster scan can be selected. The firmware has been modified for us by Optech in order to increase the scanning speed. Each range measurement contains range, elevation, azimuth, returned intensity, measurement status, and a timestamp.

We have also developed a LIDAR simulator to test the effects of different sensor noise levels, scan patterns, and scan control, and to conduct experiments without the constraints of the physical testbed. This simulator allows the definition of multiple scan windows with several scan patterns (raster, spiral, rosette, Lissajous) and variable resolutions. The relative motion of the observed target spacecraft may also be specified in the simulator.

### 4.3 Pose acquisition

The Pose Acquisition module uses 3D data from the LIDAR along with the model of the observed satellite to estimate its pose without using any prior information or constraints. The main idea is to apply 3D binary template matching to the data [10]. The grid elements of a 3D template are called *voxels* and each such element in a *voxel grid* represents a small distinct region of space and can be assigned a binary value to indicate whether that region is *empty* or *occupied*. The resolution of the voxel grid is relatively coarse, a benefit of which is to reduce the size of the pose search space by masking high frequency details. As the satellite can be positioned arbitrarily, a pure template matching approach would require a separate template for each possible pose. The approach described here is to exploit the structure of the object to resolve a subset of the pose parameters, and to apply 3D binary template matching over the reduced space of the remaining free pose parameters.

The objective is to determine a rigid transformation  $\mathbf{X}$ , generally comprising 3 rotations and 3 translations, which aligns a surface model  $\mathbf{M}$  with the sensed data  $\mathbf{P}$  of the satellite. The satellite can be positioned arbitrarily within the sensor-centric coordinate system  $\mathbf{U}$ , and the sensed data is a sparse cloud of 3D points that sample its surface at arbitrary locations. The solution has two distinct phases, each of which solves a distinct subset of the six free degrees-of-freedom (*dofs*) of the pose. The first phase is motivated by the observation that many satellites, such as the Radarsat, have an elongated structure. We assume that the sensed points are distributed evenly enough along the surface of the satellite to capture this elongation. The vector  $\mathbf{v}$  that describes the major axis can be efficiently and robustly determined by Principle Component Analysis (PCA). All points in  $\mathbf{P}$  are first translated by  $\mathbf{T}$  so that the centroid of the transformed point set  $\mathbf{Q}$  falls at the origin. Next the covariance matrix  $\mathbf{C}$  is generated for  $\mathbf{Q}$  as

$$\mathbf{C} = \begin{pmatrix} \sum x^2 & \sum xy & \sum xz \\ \sum yx & \sum y^2 & \sum yz \\ \sum zx & \sum zy & \sum z^2 \end{pmatrix}$$

where the summations are taken over the entire point set. The vector  $\mathbf{v}$  that points in the direction of the major axis of elongation of  $\mathbf{Q}$  (and thus  $\mathbf{P}$ ) is determined as the eigenvector corresponding to the maximum eigenvalue of  $\mathbf{C}$ . The final step of phase one is to identify the two rotations that align  $\mathbf{v}$  with  $\mathbf{U}_x$ . These two rotations are combined into the transform  $\mathbf{R}_{yz}$  and applied to the translated point set  $\mathbf{Q}$ .

The PCA method has been demonstrated to have a degree of robustness, so that a small number of spurious outliers that may result from background scene elements in the experimental system do not seriously skew the result. It is also not necessary to sense over the complete structure of the satellite to correctly identify the major axis, as the elongation of the satellite is evident in local regions.

Following this first phase, there still exist 4 unresolved dofs: the rotation around  $\mathbf{U}_x$  and all three translations. These are determined in the second phase using a correlation approach, which is essentially an exhaustive 3D template matching over the remaining 4 dofs. Let the function  $\mathbf{V}(\mathbf{M})$  denote the quantization of surface model  $\mathbf{M}$  onto a voxel grid, such that all voxels that intersect with the surface of  $\mathbf{M}$  will have the *occupied* value, and all other voxels will have the *empty* value. We define the *voxel occupancy* as the set of occupied voxels of  $\mathbf{V}(\mathbf{X}\mathbf{M})$  for a given pose  $\mathbf{X}$  of model  $\mathbf{M}$ .

Let  $\mathbf{M}$  be initially positioned in a canonical pose within  $\mathbf{U}$  such that its major axis is aligned with  $\mathbf{U}_x$ , its minor axis is aligned with  $\mathbf{U}_y$ , and its centroid is located at the origin. In preprocessing,  $\mathbf{M}$  is rotated around  $\mathbf{U}_x$  to  $n$  distinct pose values. The voxel occupancy of each rotation is calculated and stored in association with its rotation value. The voxel occupancies are therefore essentially 3D binary templates.

At runtime, phase one is first executed so that the point set is centered at the origin and its major axis is aligned with  $U_x$ . The point set is next quantized into the initially empty voxel grid, creating a binary 3-D image of the sensed data. Each of the voxel templates generated during preprocessing are then correlated with the voxel grid, at all possible locations. The template location with the highest correlation value indicates the rotation around  $U_x$ , and the 3 translation values of the satellite pose, within the accuracy of the voxel resolution.

This method has been demonstrated to be efficient, executing in a few seconds, and reliable. One limitation is that it applies only to elongated objects. For those satellites that are not elongated, it may be possible to apply a strategy that considers other global properties, such as symmetries, to satisfy the axis alignment of phase one. It may also be efficient to apply the template matching approach of phase two to resolve 5 free dofs, if it were only possible to resolve one dof in phase one.

#### 4.4 Pose estimation

After the initial pose of the satellite has been determined, the model based tracking mode is invoked next and initialized with this estimate. Tracking operates with high precision and a high update rate by matching the satellite model with 3D data. During tracking the pose is determined by iteratively matching 3D data with the model using a variation of the Iterative Closest Point algorithm (ICP) [2]. Our implementation of this algorithm consists of the following steps:

1. Selection of the closest points between the data set and the model in the expected pose
2. Rejection of outliers
3. Computation of geometrical registration between matched data points and the model
4. Application of geometrical registration to the data
5. Termination of the iterations after stopping criterion is reached.

The algorithm iterates over steps 1-4 until the stopping criterion (convergence and/or reaching the maximum allowed number of iterations) is met. The number of iterations required to reach the minimum depends on the difference between the expected and the actual pose. The expected pose is predicted using a pose tracker that estimates both linear and angular velocities, and applies the correction to the model pose. This predictor significantly reduces the number of iterations and thus reduces the processing time.

Detection of the closest points between the model and the data is the most computationally intensive task in ICP as it involves computing distances for each combination of data points and model features. The complexity is  $O(NM)$ , where  $N$  is the number of data points,  $M$  number of model points, and different model representations and acceleration schemes have been used to reduce it [9, 11]. Grouping model points into simple shapes allows using closed form solutions for computing distances [15]. K-d trees have been used to reduce the number of distance computations for models represented as points or meshes. Our technique eliminates all the distance computations from the on-line phase by computing them in advance off-line, and storing them in a structure that allows fast access. This however comes at a price of having to store the data and/or reduce the resolution of the distances.

The model based pose tracking does not require detecting high level features in the scene and matching them with the model features, and re-establishes correspondences between the model and data points at each iteration. This significantly reduces its sensitivity to partial occlusions and local loss of data. An adaptable gating mechanism eliminates outliers that are not part of the model. Any sampling pattern can be used for pose tracking and it is not necessary to scan any specific region of the observed satellite. However, a sufficient number of samples must be obtained and their location on the satellite shape must constrain the model alignment. Some parts of the satellite may not be accurately represented in the 3D model used for processing, e.g., surfaces covered with loosely fitting thermal blankets or articulated components in unknown orientations. Directing the LIDAR to scan regions that provide the most useful information (e.g., spatial constraints, stability, and accurate representation in the model) improves the pose estimation accuracy.

#### 4.5 Target satellite tracking

The Target Tracker module filters poses provided by the Pose Tracking module and maintains a current estimate of the satellite pose. Additionally, it selects windows for scanning and predicts the satellite pose for the next LIDAR scan. The data processing is shown in Figure 4.

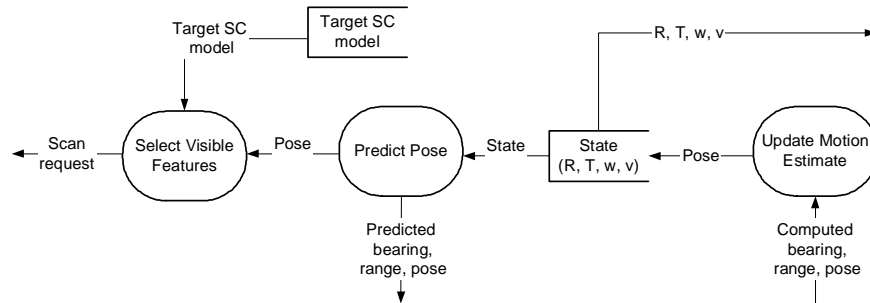


Figure 4: Target Tracker module.

The currently implemented motion model assumes that the relative linear and angular velocities between the satellite and the sensor are constant, and uses an  $\alpha$ - $\beta$  filter to fuse new measurements. More complex motion models and state estimators can be used as well, and the Pose Predictor predicts the spacecraft pose for the next LIDAR scan.

During pose tracking, rather than sampling the whole surface, the LIDAR scans selected regions on the satellite surface in order to minimize the scan time and obtain the most useful information for accurate estimation. The scan locations and sizes are selected off-line and stored with the satellite model. These locations typically include rigid structures, whose positions are accurately represented in the model. Experiments with different scan strategies (e.g., sparseness, edges, corners, surfaces, and combinations of these) have been performed and are summarized in the following section. While the system is tracking, the satellite model is placed in the pose predicted for the next scan and only those regions that are visible to the LIDAR are selected for scanning. Additional optimization involving the distribution of these regions is also possible. The window size is selected dynamically on the basis of the information stored in the model and distance.

## 5 EXPERIMENTS

The prototype model based vision system has been integrated with a commercial time-of-flight LIDAR, ILRIS-3D, from Optech, and with a LIDAR simulator. The system was tested using a moving scaled satellite replica, Radarsat-2, in the MDA Space Vision laboratory, illustrated in Figure 2.

The objective of the experiments was to characterize the main limitations and trade-offs of the system under development. It should be noted that experiments were conducted with commercial hardware (LIDAR and processors), which were not representative of space systems. On-going projects address the integration of space equivalent hardware (LIDAR, processor boards) and software (real time operating system) into the experimental testbed.

### 5.1 Testbed description

A photograph of the MDA Vision testbed is shown in Figure 5. The setup includes two industrial robots, both of which are Fanuc M710iW, with 6 degrees of freedom each. One of the robots holds a replica of a satellite, Radarsat-2 at approximately 1:5 scale, and the other robot holds an ILRIS-3D LIDAR sensor. The robots are fully calibrated and they can be programmed to follow predefined trajectories allowing testing of the vision system performance. They can also operate under closed loop control using the vision system tracking modes. The workspaces of both robots overlap and the maximum separation between the replica and the LIDAR is 6 m. Tests at longer distances are possible, albeit without the ability to perform a continuous motion to contact. Testing is performed under illumination that simulates direct Sun light and Earth albedo. The satellite models used in the tests have been manufactured using actual space surface materials to create realistic imaging effects.



Figure 5: MDA Space Vision testbed with a scaled replica of Radarsat-2 (left) and LIDAR, ILRIS 3D (right)

## 5.2 Pose acquisition

The Pose Acquisition module assumes that the 3D data will be approximately uniformly sampled on the satellite surface. A higher sampling density is likely to provide more accurate and reliable data; however, this will require longer scanning and processing times. An increased scan time will in turn lead to the creation of motion artifacts (e.g., motion skew) if both spacecrafts are moving. In the following experiments we attempted to determine the effects that the number of range measurements have on the performance of pose acquisition, with the objective of minimizing the number of measurements necessary.

We have generated several different trajectories for the Radarsat-2 replica and collected 110 dense 3D data sets (uniform raster scan) by placing the replica in different orientations at approximately the same distance of 5 m. Each scan was performed with the same density and included from 15,000 to 60,000 data points from the replica depending on the orientation. Any measurements that fell on the background walls were removed by simple range gating. The original 3D data was resampled by randomly discarding from 10% to 99.99% of the data. The resulting point cloud was then processed by the pose acquisition algorithm. Example scans at different resolutions with identified major axes are shown in Figure 6 and the results are summarized in Figure 7.

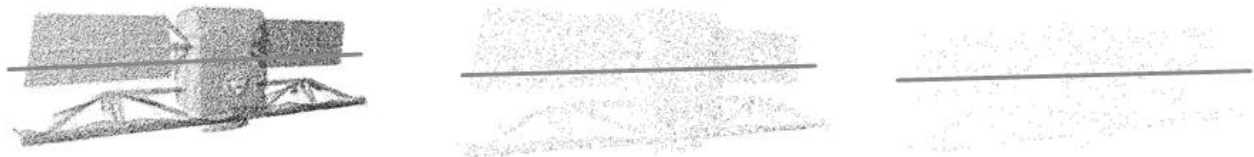


Figure 6: Major axis computed for 3D data sets sampled at different resolutions (left ~ 20k points, middle ~ 3k, right ~ 300)

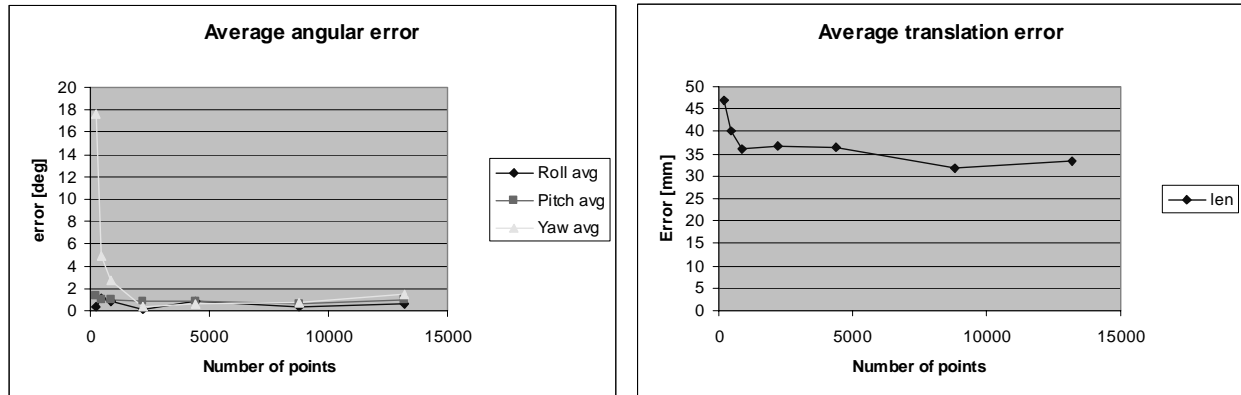


Figure 7: Pose acquisition errors

The average pose acquisition errors are almost constant for more than 2,000 samples and significantly increase for less than 500 measurements for successful runs. The algorithm failures were caused by the geometric symmetry of the Radarsat, and by singular views. The only difference between the front and the back is the presence of a docking interface at the front. This symmetry has resulted in errors for less than 2,000 samples. For less than 500 measurements we have also observed the effects of top-down symmetry. The singular views include the side and bottom views where there is not enough information for unique classification.

The pose acquisition time is in the range of several seconds for a data set of 3,000 points on a PIII processor.

An analysis of the failure modes suggests that the current pose acquisition algorithm could be augmented to function effectively with fewer than 2,000 points by subsequently performing a detailed check of local areas (possibly with a subsequent scan) to remove potential ambiguities in the pose. Location of such a scan could be selected using a similar technique as is used in pose tracking. Other satellite shapes might have different ambiguities and singular views, which could be characterized using the same experimental process.

### 5.3 Pose tracking

The performance of pose tracking has been tested using data from the following 3 sources: ILRIS range sequences of various mockups mounted on a stationary robot and moved between positions; ILRIS scans captured while the mockup was in motion; and from a LIDAR simulator. Each of these data sets allowed different modes of analyses, with the simulator being the most flexible and providing the most accurate ground truth, and the scanning of a moving replica providing realistic effects of motion blur but with only limited ground truth information.

#### 5.3.1 Simulator data

The simulator data was used to test effects of the LIDAR accuracy on the pose tracking accuracy for different scan strategies. Table 1 lists the settings for the range, azimuth, and elevation errors used in these experiments. The best results have been obtained for dense scanning of the spacecraft; however, this required a significantly longer processing time when compared to sparse scanning. Among the window scanning strategies, the best results were obtained for dense sampling around corners with sparse sampling of the complete surface.

Case	Range error, $1 \sigma$	Azimuth angle error, $1 \sigma$	Elevation angle error, $1 \sigma$
Error1	1cm	0.1mrad	0.1mrad
Error2	2cm	0.1mrad	0.1mrad
Error3	2cm	1mrad	1mrad

Table 1. Rangefinder simulator error parameters for various cases: Error1, Error2 and Error3.

Figure 8 shows example results obtained for 1) dense sampling, 2) sparse sampling, 3) corners, 4) edges, 5) corners with sparse sampling, and 6) edges with sparse sampling. The data sets consisted of approximately 50,000 data points for the dense data set and 1,000 for the others. The scanning windows were defined around the object corners, edges and optionally included sparse sampling of the surface.

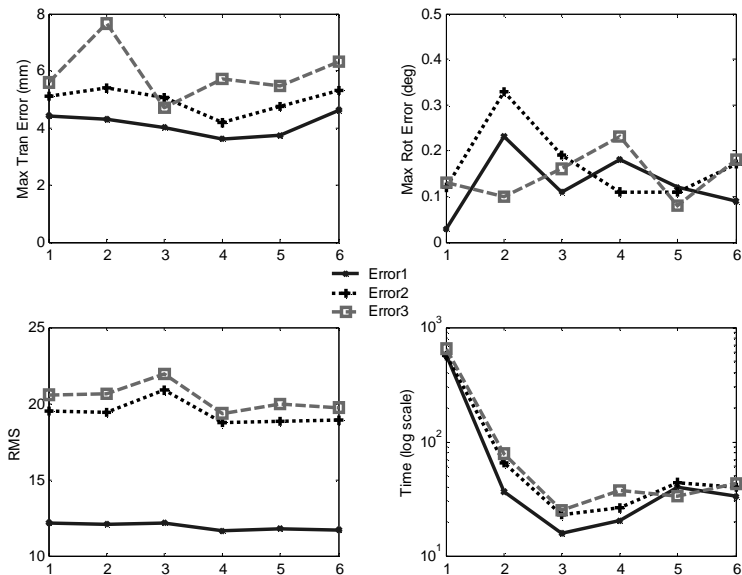


Figure 8: The effect of feature selection on ICP error, RMS and time for different error parameters with simulated Radarsat at a near distance (100, -230, 8000, 25, 20, -30): 1 for dense, 2 for sparse, 3 for corners, 4 for edges, 5 for corners with sparse and 6 for edges with sparse.

### 5.3.2 Sequences of static scans with ILRIS

Results of pose tracking using windows located at corners and sparse sampling of the surface are shown in Figure 9. The mockup was moving by exactly 30 mm in the Z direction between the scans and approximately 1,000 range points were obtained for each scan. The  $\alpha$ - $\beta$  tracker was used in these experiments. The estimated translation is consistent with the measurements from the robot and the error is below 10 mm; the residual changes in the orientation are below 1 degree. The RMS error is below 30 mm.

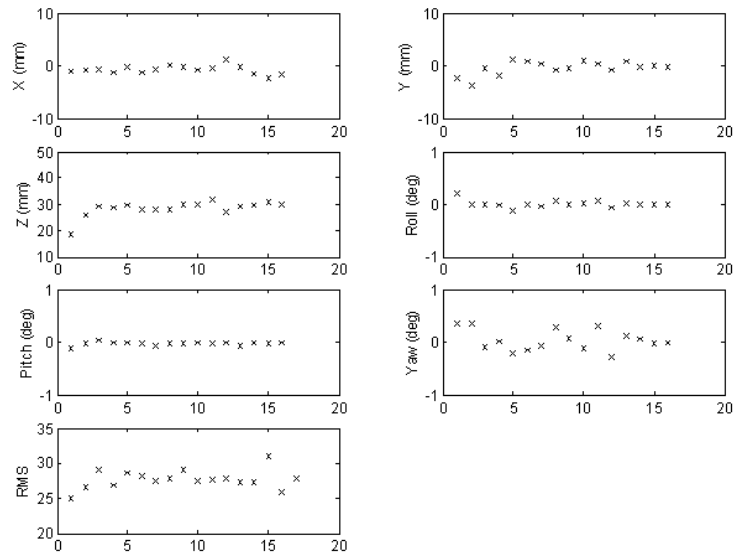


Figure 9: The change of pose between frames real Radarsat sequence when both sparse object and dense corners are scanned with tracker parameter  $\alpha=0.8$  for a fixed 30mm translation in Z direction.

### 5.3.3 Pose tracking for a moving replica

Position and orientation estimates of the Radarsat-2 replica that was scanned and tracked during motion is shown in Figure 10. Between 2,000 and 3,000 measurements were obtained for each scan.

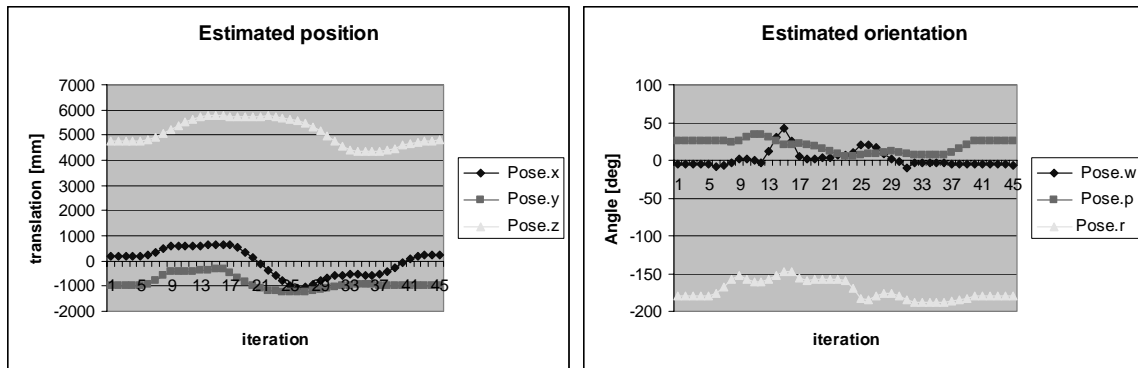


Figure 10: Estimated position and orientation

The pose tracking processing time is in the range from 50 to 200 ms on a PIII processor, depending on the initial misalignment and termination conditions. It is possible to trade-off accuracy and efficiency by setting the maximum number of iterations of the algorithm.

## 6 CONCLUSIONS

This paper presents an overview of algorithms and the architecture of a proof-of-concept vision system for the model-based pose estimation of satellites during rendezvous and docking. The system has been integrated with a commercial time-of-flight LIDAR, and a LIDAR simulator, and tested in laboratory conditions; selected test results are also presented.

Tests of the integrated proof-of-concept system indicate the feasibility of a LIDAR based model based vision system that is suitable for autonomous rendezvous and docking in space. Such a system will not require retro-reflectors or visual

targets for its operation and will rely on known 3D models of the satellites of interest. One of the LIDAR limitations is the sequential range data acquisition and the total scan time. Our pose acquisition algorithm operates reliably with a few thousand sparsely sampled points, instead hundreds of the thousands of points that are generated by dense sampling. Our pose tracking algorithms guide the LIDAR to densely scan selected regions only and they provide accuracy comparable to the use of complete dense scans at a fraction of the time necessary to collect and process the data.

The current development work focuses on advancing the system to space equivalent hardware (LIDAR and processor) and software environments (real-time operating system), testing the performance using other satellite replicas, and extensions of the algorithms.

The described work has been funded, in part, by the Canadian Space Agency under the Space Technology Development Program.

## 7 REFERENCES

- 1 Besl, P. & N. McKay: A Method for Registration of 3-D Shapes. IEEE PAMI, vol. 14, no. 2, 1992, pp. 239-256.
- 2 F. Blais: Review of 20 years of range sensor development. J. of Electronic Imaging 13(1), 231– 240 (Jan 2004).
- 3 Chin Seng Chua and Ray Jarvis. Point signatures: A new representation for 3d object recognition. Intl. Jour. Comp. Vis., 25(1):63–85, 1997.
- 4 Fred Clark, Peter Spehar, Jack Brazzel, Heather Hinkel: Laser based Relative navigation and Guidance for Space Shuttle Proximity Operations. Guidance and Control 2003 Conference AAS Vol.113, p. 171-86
- 5 Creamer, Glenn; Pipitone, Frank; Gilbreath, Charmaine; Bird, Dexter; Hollander, Sam: NRL technologies for autonomous inter-spacecraft rendezvous and proximity operations. AAS v 115. 2003.
- 6 Wigbert Fehse: Automated Rendezvous and Docking of Spacecraft. Cambridge University Press, 2003.
- 7 Michael Greenspan, Guy Godin: A Nearest Neighbor Method for Efficient ICP. 3DIM01 : Proceedings of the 3rd International Conference on 3-D Digital Imaging and Modeling, Quebec City, Quebec, Canada, May, 2001.
- 8 Michael A. Greenspan. Geometric probing of dense range data. IEEE Trans. PAMI, 24(4):495–508, April 2002.
- 9 Michael Greenspan, Limin Shang, Piotr Jasiobedzki: Efficient Tracking with the Bounded Hough Transform. CVPR 2004
- 11 Hihara Hiroki, Ken Nagai, Hiroaki Miyoshi, Masashi Uo, Isao Kawano, Masaaki Mokuno: Development of the Rendezvous RADAR for the ETS-VII. AIAA-98-1297, pp. 400-407.
- 12 S. Hollander. Autonomous space robotics: Enabling technologies for advanced space platforms. In AIAA Space 2000 Conference, 2000.
- 13 Howard, Richard T., Bryan T.C., Book, Michael L.: The Video Guidance System – a Flight Proven technology. AAS Guidance and Control 1999, pp. 281-298.
- 14 Jasiobedzki P, Talbot J, Abraham M: Fast 3D pose estimation for on-orbit robotics. International Symposium on Robotics, ISR 2000 Montreal, Canada, May 14-17, 2000.
- 15 P. Jasiobedzki, MA. Greenspan, G. Roth. Pose determination and tracking for autonomous satellite capture. In iSAIRAS 2001.
- 16 Andrew Edie Johnson and Martial Hebert. Efficient multiple model recognition in cluttered 3-d scenes. In Proceedings of Computer Vision and Pattern Recognition, pages 671–676, May 1998.
- 17 Isao Kawano, Hiroshi Ueno, Yoshiyuki Ishijima, Tadashi Adachi, Takahiko Iijima: Study on Laser Rangefinder for Non-cooperative Rendezvous. i-SAIRAS 2003, NARA, Japan, May 19-23, 2003.
- 18 Nimmelman M., Tripp J.: Spaceborne scanning lidar system. SPIE vol 5798 Spaceborne Sensors II, March 2005.
- 19 Optech ILRIS 3D <http://www.optech.ca/prodilris.htm>
- 20 F. Pipitone W. Adams: Tripod Operators for Recognizing Objects in Range Images: Rejecting Library Objects Without Explicit Models, IEEE Proc. Robotics and Automation Conference, Nice, France, May 12-14, 1992.
- 21 M.E. Polites. An Assessment of the Technology of Automated Rendezvous and Capture in Space. NASA/TP—1998–208528.
- 22 RVS <http://www.jena-optronik.de/sensors/rvs.html>.
- 23 Samson, C., English, C., Deslauriers, A., Christie, I., Blais, F., Ferrie, F. Neptec 3D Laser Camera System: From Space Mission STS-105 to Terrestrial Applications, Canadian Aeronautics and Space Journal. June 2004.
- 24 Simon, D.A.; Hebert, M.; Kanade, T.: Real-time 3-D Pose Estimation Using a High-Speed Range Sensor, IEEE International Conference on Robotics and Automation, 1994.